Genes & Diseases (2026) 13, 101843

Available online at www.sciencedirect.com

ScienceDirect

journal homepage: www.keaipublishing.com/en/journals/genes-diseases

FULL LENGTH ARTICLE

Transcriptional rewiring by enhancer methylation in CBFA2T3-GLIS2—driven pediatric acute megakaryoblastic leukemia

Samrat Roy Choudhury [a,*], Akhilesh Kaushal [a,e], Pritam Biswas [a,e], Cory Padilla [b], Jay F. Sarthy [c], Arundhati Chavan [a], Giselle Almeida Gonzalez [a], Soheil Meshinchi [d], Jason E. Farrar [a]

[a] *Pediatric Hematology-Oncology, Department of Pediatrics, Arkansas Children's Research Institute, University of Arkansas for Medical Sciences, Little Rock, AR 72202, USA*
[b] *Cantata Bio, Scotts Valley, CA 95066, USA*
[c] *Seattle Children's Research Institute, Seattle, WA 98105, USA*
[d] *Translational Science and Therapeutics Division, Fred Hutchinson Cancer Center, Seattle, WA 98109, USA*

Received 29 March 2025; received in revised form 11 June 2025; accepted 30 June 2025
Available online 6 September 2025

KEYWORDS
Acute megakaryoblastic leukemia;
Acute myeloid leukemia;
CBFA2T3-GLIS2;
cis-regulatory elements;
DNA methylation;
Enhancer

Abstract Resistance to chemotherapy and subsequent relapse remain the primary challenge in pediatric acute myeloid leukemia (pAML), particularly in CBFA2T3-GLIS2 (C/G) fusion-positive acute megakaryoblastic leukemia. Here we demonstrate that the C/G fusion drives extensive DNA methylation changes and oncogenic enhancer activation at cis-regulatory elements (CREs), reshaping gene expression. This multi-omics analysis reveals a distinct hypermethylation pattern at promoters of up-regulated genes in C/G$^+$ pAML across patient samples ($n = 24$) and representative cell lines, notably enriched in adhesion-related, TGFβ, or Wnt signaling pathways. Hypermethylated regions adjacent to transcription start sites (TSS) maintain open chromatin with H3K27ac enrichment, supporting a mechanism of *de novo* chromatin looping and active transcription in a non-canonical manner. Additionally, C/G fusion binding near the DNA methyltransferase 3B (*DNMT3B*) promoter correlates with elevated *DNMT3B* expression, implicating its role in aberrant DNA methylation changes at CREs. This study elucidates the epigenetic mechanisms driving C/G$^+$ pAML, showing how the fusion reshapes chromatin and DNA methylation landscapes by impacting the expression (and likely activity) of epigenetic

* Corresponding author. Tel.: +1501 364-7531.
E-mail address: sroychoudhury@uams.edu (S.R. Choudhury).
Peer review under responsibility of Chongqing Medical University.
[e] These authors contributed equally to this work.

https://doi.org/10.1016/j.gendis.2025.101843

modifiers like DNMT3B. Functionally, DNMT3B inhibition enhances apoptotic sensitivity to BCL2 blockade, indicating that targeting DNMT3B may overcome apoptotic resistance in C/G$^+$ leukemic cells and offer a therapeutic strategy for this high-risk subtype.

Introduction

Acute myeloid leukemia (AML) is a highly heterogeneous clonal neoplasm arising from hematopoietic stem cells (HSCs), characterized by genetic and epigenetic alterations that drive the unchecked proliferation and infiltration of immature myeloid cells across multiple organs.[1,2] Acute megakaryoblastic leukemia (AMKL), more common in pediatric AML (pAML), involves the uncontrolled proliferation of megakaryoblasts (MK), the precursors of platelets.[3] While most AMKL cases in pAML patients with Down syndrome have a favorable survival rate (>80%), patients with non-Down-syndrome AMKL (*de novo* AMKL) face poor outcomes, with only 34% overall survival.[4] Among *de novo* AMKL cases, a particularly high-risk subgroup limited to young children (<3 years) is defined by the presence of the CBFA2/RUNX1 partner transcriptional co-repressor 3 (CBFA2T3)-GLIS family zinc finger 2 (GLIS2) (C/G) oncofusion, also observed in certain non-AMKL pAML cases.[5–7] This fusion confers resistance to chemotherapy; C/G$^+$ patients are generally refractory to treatment, with high relapse rates.[8,9] Although induction therapy temporarily achieves remission in approximately 50% of C/G$^+$ cases, over 90% of these patients retain minimal residual disease, contributing to frequent relapse and poor event-free survival. Salvage therapy after relapse is often ineffective, resulting in an overall survival rate below 15%.[6,10–13]

At the molecular level, the C/G fusion exerts a potent oncogenic 'hit' that significantly alters leukemic properties, leading to the up-regulation of the E−26 transformation-specific transcription factor-related gene (ERG) and down-regulation of GATA-binding factor 1 (GATA1).[14,15] The overexpressed ERG, together with C/G, drives the formation of *de novo* super-enhancer (SE) elements, establishing a feedforward loop that amplifies gene expression, including genes like *KIT*.[14,16] Notably, these C/G-induced SEs are situated far from canonical binding sites for CBFA2T3 or its typical partners, such as GATA1, TAL1, or RUNX, observed in MK progenitors,[14,17] thereby contributing to dysregulated gene expression.

Additionally, the C/G fusion binds to proximal promoter regions of DNA methyltransferase 3B (DNMT3B), enhancing their expression and potentially explaining the genome-wide hypermethylation observed in C/G$^+$ cells.[18,19] Abnormal DNMT3B activity, which induces CpG island hypermethylation, has been shown to influence HSC fate and sustain disease-specific enhancer activities.[20,21] However, the precise impact of hypermethylation at cis-regulatory elements (CREs) on transcriptional programs in C/G$^+$ pAML remains unclear. Here, we present an integrative multi-omics approach to assess how DNA methylation and chromatin modifications interact to regulate the enhancer-driven transcriptional program in C/G$^+$ pAML.

Materials and methods

Patient samples and cell lines

Primary pAML samples (n = 75) from the Children's Oncology Group clinical trials (AAML0531, AAML1031, and AAML03P1) were analyzed and compared with normal bone marrow mononuclear cells (NBM) from healthy donors under 18 years old (n = 10; Table S1). The study also included two C/G$^+$ cell lines (M07e and WSU-AML) and three non-C/G AML cell lines (KG1A, KASUMI-1, and ME-1), as well as cord blood-derived CD34$^+$ HSC and MK progenitors. Details of the culture conditions are provided in the supplementary information.

DNA methylation analysis

We analyzed DNA methylation data from patient-derived samples and NBM isolates, generated using the Illumina MethylationEPIC V1.0 BeadChip array (Illumina Inc., USA) and deposited in public databases (GSE124413 and GSE190931). For primary cells and AML cell lines, DNA methylation assays were conducted using the Illumina MethylationEPIC V2.0 array platform, and the resulting data were analyzed. Detailed information on DNA methylation data processing and annotation can be found in the supplementary information. CpG sites with a ≥10% increase in DNA methylation in AML samples (patients or cell lines) compared with controls (NBM for patients or HSC/MK for cell lines) were classified as hypermethylated, while those with a ≥10% decrease were classified as hypomethylated. Additionally, we performed reduced representation bisulfite sequencing (RRBS) in M07e cells per our previously published protocol,[22,23] to identify differentially methylated regions (DMRs) following functional knockout (KO) of DNA-methyltransferase 3B (*DNMT3B*), compared with wild-type (WT) M07e cells (see supplementary information for details). Consistent with the MethylationEPIC arrays, we considered an absolute change of ≥10% in DNA methylation in DMRs to be significant between KO and WT cells.

RNA sequencing

The transcriptome profiles of C/G$^+$ pAMKL and NBM samples were obtained from published RNA sequencing datasets available at dbGAP (accession # phs000465.v19. p8).[10] For primary cells and AML cell lines, RNA sequencing libraries were prepared using our previously published protocol.[22] Detailed information on the processing and analysis of RNA sequencing data can be found in the supplementary information.

Integration of DNA methylation and expression

Genes with an average absolute Δβ-value of ≥10% at their promoters or gene bodies, calculated from differentially methylated CpG sites (DMCs) between AML samples and controls, were designated as differentially methylated genes (DMGs). We then integrated these DMGs with corresponding differential expression profiles ($|\log_2$ fold change$| \geq 1$). This intersection of DMGs and differentially expressed genes yielded four distinct gene clusters: i) hypermethylated and up-regulated (hyper—up), ii) hypermethylated and down-regulated (hyper—down), iii) hypomethylated and up-regulated (hypo—up), and iv) hypomethylated and down-regulated (hypo—down).

Identification of differentially methylated chromatin states in C/G$^+$ pAML

Chromatin immunoprecipitation-sequencing data for four chromatin marks (H3K4me1, H3K4me3, H3K27ac, and H3K27me3) in M07e cells were retrieved from a previous study.[14] These datasets were processed in-house to annotate chromatin states at CREs using a multivariate hidden Markov model (ChromHMM)[24] with a 10-state configuration. The model followed established definitions and emission parameters (see details in supplementary information).[25] Differential DNA methylation data were then integrated with the annotated chromatin states to identify overlaps between hyper- and hypo-methylated CpGs and regulatory chromatin states (defined as *methylated chromatin states*) using BEDTools.[3] Visualizations of epigenetic marks for selected genes were generated using the Integrative Genome Viewer (IGV).[26]

Determination of chromatin accessibility across differentially methylated chromatin states

Chromatin accessibility in M07e cells was assessed using the assay for transposase-accessible chromatin with sequencing (ATAC-sequencing) data obtained from a previously published study.[16] ATAC-sequencing peaks were identified with MACS2.[27] Differentially enriched open chromatin regions in M07e cells were compared with those in CD34$^+$ HSCs and integrated with differentially methylated chromatin states using BEDTools.[3] Significant overlaps were defined as regions with ≥50 bp overlap between differentially methylated chromatin states and open chromatin regions.

High-throughput promoter capture chromosome conformation capture techniques

Promoter capture Hi-C (PCHi-C) was used to analyze long-range chromosomal interactions between promoters and distal regulatory regions in C/G$^+$ M07e cells, compared with HSCs.[28] Libraries were prepared using the Dovetail® Pan Promoter™ Assay (Catalog #35013E, Cantata Bio), following the manufacturer's protocol. Details of the PCHi-C sequencing and data analysis pipeline are provided in the supplementary information. Genome-wide binding of the CCCTC-binding factor (CTCF) in M07e cells was mapped using CUT&RUN sequencing following established protocols.[29,30] This analysis enabled the identification of CTCF-guided and non-CTCF-guided *de novo* promoter-interacting loops. These interactions were further integrated with differential DNA methylation data to investigate the role of DNA methylation in shaping complex three-dimensional genome organization.

Determining the binding distribution of the C/G fusion

CUT&RUN sequencing was conducted to examine the binding and distribution of CBFA2T3, GLIS2, and histone modifications (H3K4me3, H3K27ac, and H3K27me3) at C/G binding sites in C/G$^+$ M07e cells and C/G$^-$ K562 cells following previously published protocols.[29,30] An N-terminal CBFA2T3-specific antibody was used to detect CBFA2T3 binding, and a GLIS2-specific antibody recognizing an epitope within amino acids 260—310 was employed to detect the center of human GLIS2 binding (GLIS2^{Cent}). Additionally, an N-terminal GLIS2-specific antibody, which lacks a target in the C/G fusion, served as a negative control for GLIS2 binding. Regions exhibiting peaks common to both the N-terminal CBFA2T3 and GLIS2 (aa 260—310) antibodies were designated as C/G-binding sites.

Generation of DNMT3B KO M07e cells via CRISPR-Cas9 lentiviral transduction

To generate *DNMT3B* KO M07e cells, we employed CRISPR-Cas9-mediated genome editing via lentiviral transduction. The single-guide RNA (sgRNA) targeting *DNMT3B* was designed using the Cas-Designer program, with potential off-target sites and mismatch profiles assessed using the Cas-OFFinder tool from CRISPR RGEN.[31,32] The sgRNA, targeting exon 6 of *DNMT3B*, was individually cloned into a lentiviral vector under the control of a human U6 promoter, while SpCas9 and a puromycin resistance gene were co-expressed under an EFS promoter. Lentiviral particles were generated by transfecting HEK293T cells with the CRISPR construct using Lenti-X™ Packaging Single Shots (VSV-G) (#631275, Takara). Viral supernatants were harvested 48 h post-transfection, filtered, and used to transduce M07e cells seeded onto Retronectin (#T202, Takara)-coated plates (10 μg/mL). Infected cells were subjected to puromycin selection (1 μg/mL) for 15 days, followed by clonal isolation via limiting dilution. Single-cell clones were screened for *DNMT3B* disruption using western blotting analysis. A non-targeting sgRNA (scramble) control was included to evaluate potential off-target effects. To assess the basal effect of *DNMT3B* loss on cell viability in the absence of drug, M07e WT and DNMT3B KO cells were seeded at equal density in 96-well plates and cultured under standard growth conditions. After 48 h, viability was assessed using the CellTiter-Glo assay (Promega) per our previous studies.[33,34] DNMT3B KO viability was normalized to the WT control, and statistical significance was determined using an unpaired two-tailed *t*-test with Welch's correction.

Assessment of chemotherapeutic sensitivity following DNMT3B inhibition

To determine the effect of DNMT3B loss on chemotherapeutic response, we assessed the sensitivity of M07e WT and DNMT3B KO cells to venetoclax, a BCL-2 inhibitor. Venetoclax was serially diluted from 25 μM to 10 nM and added to cultures in six biological replicates. After 48 h of treatment, cell viability was measured using the CellTiter-Glo luminescent cell viability assay (Promega). Luminescence was recorded using an Agilent BioTek Gen5 microplate reader (Winooski, VT, USA), and the half-maximal inhibitory concentration (IC_{50}) was calculated using nonlinear regression in GraphPad Prism v7.0 (Boston, MA, USA). For apoptosis analysis, M07e DNMT3B KO cells were treated with 0.145 μM venetoclax, one-fold below the IC_{50} determined for these cells (0.29 μM), for 48 h. Cells were stained with annexin V-FITC and propidium iodide (PI) using a commercial apoptosis detection kit (Thermo Fisher Scientific) and analyzed on a BD LSRFortessa 4-laser, 16-color flow cytometer. Cells were classified as viable (annexin V^-/PI^-), early apoptotic (annexin V^+/PI^-), late apoptotic (annexin V^+/PI^+), or necrotic (annexin V^-/PI^+), and quantified using FlowJo software (v10.8).

Statistical analysis

A two-way ANOVA was used to assess significance in the differential methylation analysis. For all additional analyses, we used either a non-parametric, two-tailed Mann–Whitney *U* test or a one-tailed Wilcoxon test, as appropriate. Statistical significance was set at a false discovery rate of <0.01 or <0.05, as indicated in the results. Selected Graphics were created using BioRender.

Results

C/G$^+$ pAML displays a distinct DNA methylation landscape

We performed genome-wide DNA methylation profiling in C/G$^+$ pAML, including both megakaryocytic (M7, $n = 9$) and non-megakaryocytic ($n = 15$) subtypes, and compared these to non-C/G *de novo* AMKL samples ($n = 51$) and NBM ($n = 10$) (Fig. 1A and Table S1). Principal component analysis of the top 5% (~36,000) most variable CpG sites revealed a clear segregation pattern between NBM isolates and C/G$^+$ pAML samples, including both M7 and non-M7 lineages (Fig. S1). We identified 91,462 DMCs common to both C/G-M7 and C/G-non-M7 samples compared with NBM, mapping to 20,580 DMGs (Fig. 1B). Similarly, comparison of C/G$^+$ cell lines (M07e, WSU-AML) to HSCs and MK progenitors revealed 26,117 DMCs associated with 25,517 DMGs (Fig. 1C). After excluding pseudogenes and non-coding loci, intersection of these two datasets yielded 17,716 shared, protein-coding DMGs in C/G$^+$ samples across patient and cell line contexts (Fig. 1D). Region-specific analysis showed that in patient samples, 9370 DMGs were altered at promoters and 10,089 at gene bodies. In cell lines (based on M07e *vs.* HSC), 5779 DMGs were hypermethylated and 3951 hypomethylated at promoters, while 4325 were hypermethylated and 5764 hypomethylated in gene bodies. The total number of hyper-/hypomethylated genes across regions exceeds the number of unique DMGs (19,819 *vs.* 17,716), reflecting certain genes that undergo differential methylation at both promoters and gene bodies. Density plots of β-value differences (Δβ) revealed that methylation changes in patients were largely concentrated within a ±25% range across promoters, gene bodies, and intergenic regions, whereas cell lines displayed broader methylation shifts extending to ±75% (Fig. 1E–G), suggesting more extensive epigenomic remodeling *in vitro*.

To evaluate whether these methylation patterns are conserved, we performed unsupervised hierarchical clustering using the top 10% most differentially methylated DMGs (based on Δβ magnitude) stratified by genomic context. In C/G$^+$ patients, this included 947 promoter-associated and 932 gene body-associated DMGs, comprising 4418 hypermethylated and 5312 hypomethylated genes at promoters, and 3426 hypermethylated and 6663 hypomethylated genes at gene bodies (Fig. 1H). In C/G$^+$ cell lines, the corresponding promoter subset ($n = 1030$) included 5779 hypermethylated and 3951 hypomethylated genes, while the gene body subset ($n = 1017$) included 4325 hypermethylated and 5764 hypomethylated genes (Fig. 1I). Clustering analysis confirmed that C/G-M7 and C/G-non-M7 cases grouped together, distinctly separated from NBM and non-C/G AMKL subtypes. Similarly, M07e and WSU-AML clustered closely with each other, segregating from normal hematopoietic progenitors and non-C/G AML cell lines. Collectively, these findings define a conserved, lineage-independent C/G-associated methylation program enriched at both promoters and gene bodies. While both hypermethylation and hypomethylation events are observed, C/G$^+$ cell lines exhibit a modest enrichment of hypermethylation relative to primary leukemias (Tables S2 and S3), highlighting both shared and context-specific features of epigenetic dysregulation in C/G-driven leukemia.

Gene expression in C/G$^+$ pAML is associated with both canonical and non-canonical changes in DNA methylation

Previous comprehensive transcriptome profiling studies have identified C/G fusion-specific genes and pathways.[10,35] To elucidate potential epigenetic mechanisms underlying gene dysregulation in C/G$^+$ pAML, we integrated matched DNA methylation and transcriptomic data from patient samples and cell lines. Intersecting DMGs with differentially expressed genes identified 3809 unique genes in C/G$^+$ patients (Fig. 2A and Table S4), 3968 in M07e cells compared with HSCs, and 2723 in M07e compared with MKs (Fig. 2B and Tables S5 and S6). Overall, correlation between differential DNA methylation and gene expression was weak ($R^2 < 0.1$), consistent with the observation that both promoter and gene body hypermethylation or hypomethylation were associated with either gene up-regulation or down-regulation (Table S7).

Focusing on up-regulated differentially expressed genes linked to altered DNA methylation, we identified 952 promoter- and 864 gene body-associated up-regulated genes in

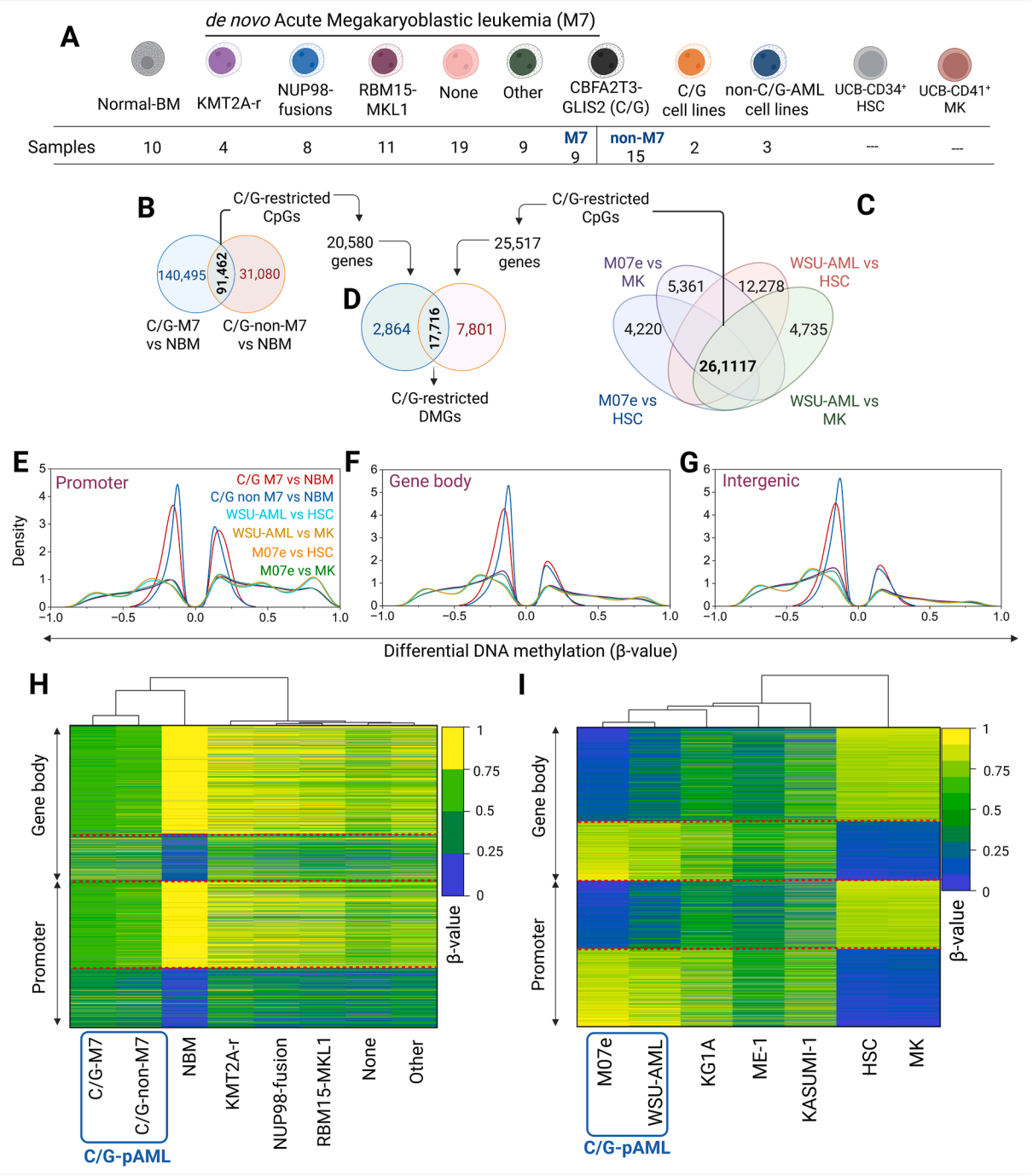

Figure 1 DNA methylation landscape of C/G$^+$ pediatric acute myeloid leukemia (AML) and cell line models. **(A)** Overview of the cohort, including all *de novo* acute megakaryoblastic leukemia subtypes ($n = 75$), compared with mononuclear cells derived from the bone marrow (BM) of non-cancer donors under 18 years of age ($n = 10$). This analysis also incorporated two CBFA2T3-GLIS2 (C/G)-positive AML cell lines (M07e and WSU-AML), three non-C/G AML cell lines (KASUMI-1, KG1A, and ME-1), as well as CD34$^+$ hematopoietic stem cells (HSC) derived from umbilical cord blood, and CD41$^+$ megakaryocytic progenitors (MK) differentiated from CD34$^+$ HSCs. **(B)** The Venn diagram illustrating differentially methylated CpGs (DMCs) shared between C/G$^+$ pediatric AML cases, representing both megakaryoblastic (M7) and non-M7 lineages, corresponding to 24,479 differentially methylated genes (DMGs). **(C)** The Venn diagram showing the overlap of DMCs between C/G$^+$ cell lines (M07e and WSU-AML) when compared with HSC and MK progenitors, identifying 33,561 DMGs. **(D)** Intersection analysis of DMGs across C/G$^+$ pediatric AML patients and cell lines, revealing 19,410 DMGs unique to the C/G fusion. **(E, G)** Frequency distribution of DMCs in C/G$^+$ pediatric AML patients (E) and C/G$^+$ cell lines (G), categorized by their genomic locations across promoters, gene bodies, and intergenic regions. **(H)** The heatmap illustrating the clustering of major *de novo* acute megakaryoblastic leukemia patients and normal BM (NBM) isolates based on DNA methylation profiles at promoters and gene bodies of C/G-restricted genes. **(I)** The heatmap of DNA methylation at promoters and gene bodies of C/G-restricted genes, comparing C/G$^+$ and non-C/G AML cell lines with HSCs and MK progenitors, demonstrating distinct clustering patterns.

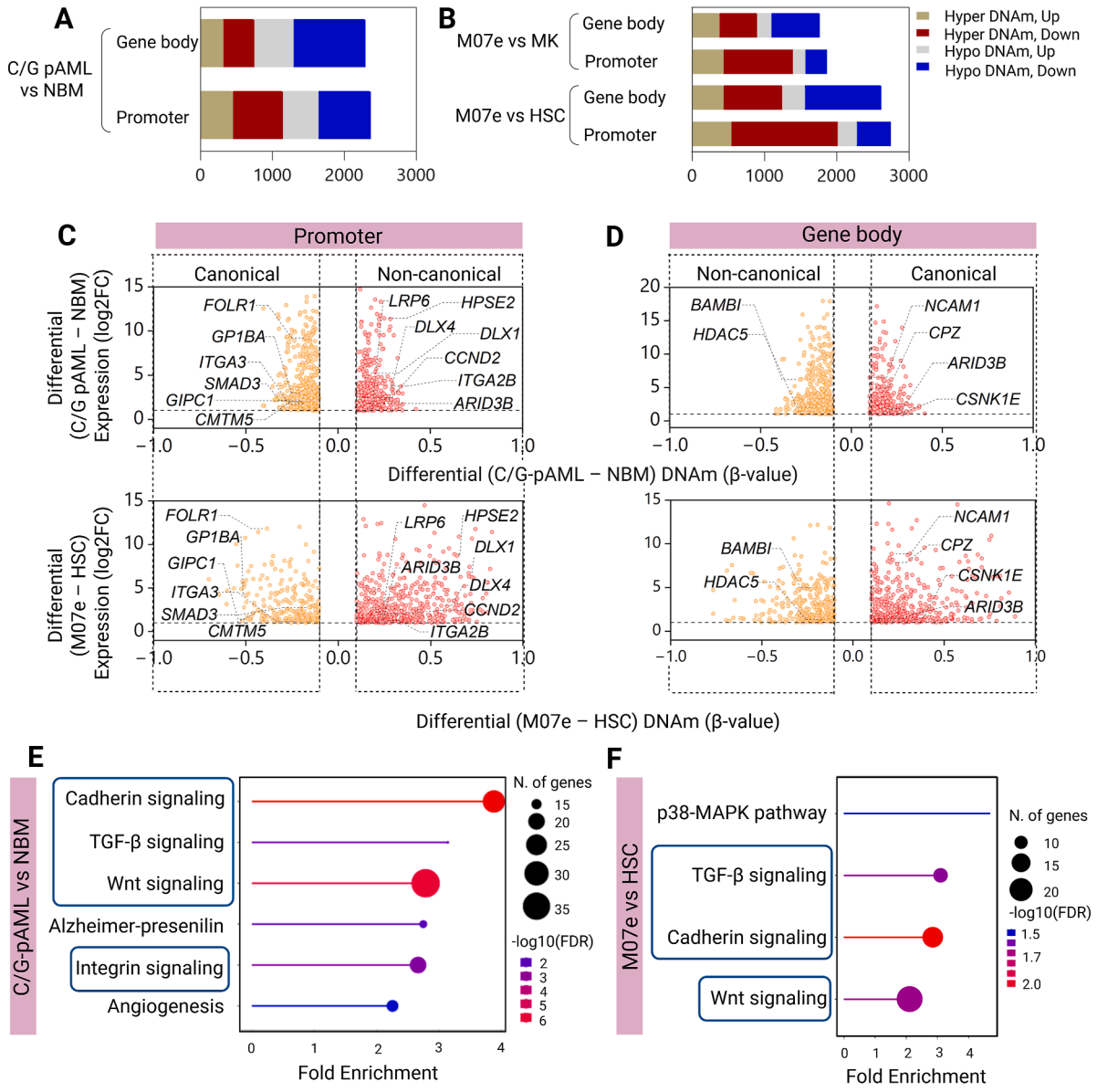

Figure 2 Relationship between DNA methylation and gene expression in C/G$^+$ pediatric acute myeloid leukemia (AML). **(A)** The stacked bar graphs illustrating the proportions of genes that are both differentially methylated (at promoter and gene body regions) and differentially expressed in CBFA2T3-GLIS2 (C/G)-positive AML patients relative to normal bone marrow (NBM) isolates. **(B)** The stacked bar graphs showing the proportions of differentially methylated and differentially expressed genes in the C/G$^+$ cell line M07e, compared with hematopoietic stem cells (HSC) and megakaryocytic (MK) progenitors. **(C, D)** The scatter plots of up-regulated genes ($\log_2$ fold change >1, $p < 0.05$) in C/G$^+$ pediatric AML patients compared with NBM isolates and in M07e cells compared with HSC. The plots display genes with either hypermethylation or hypomethylation at their promoter (C) or gene body regions (D), indicating correlations between methylation status and gene expression levels. **(E, F)** Enrichment analysis of differentially methylated and expressed genes in C/G$^+$ patients (E) and the C/G$^+$ cell line M07e (F) reveals common pathways associated with cell adhesion, TGF-β signaling, and Wnt signaling, highlighting pathways potentially impacted by C/G-specific methylation and expression patterns.

C/G$^+$ patients, and 810 and 748 such genes in M07e cells, respectively (Fig. 2C, D). We prioritized up-regulated genes for further analysis, given their potential roles in leukemogenesis and their relevance as candidate immunotherapeutic targets in C/G$^+$ pAML. Among these, several established C/G-restricted genes (*e.g.*, *FOLR1*, *GP1BA*, *CMTM5*, and *SMAD3*) demonstrated canonical inverse relationships between promoter methylation and gene expression. However, a substantial subset, including *HPSE2*, *ITGA2B*, and *DLX4*, were paradoxically up-regulated despite promoter hypermethylation, consistent with non-canonical regulatory mechanisms (Fig. 2C). A similar pattern was observed at gene bodies: while genes such as *BAMBI* and *HDAC5* were up-regulated in association with hypomethylation (non-canonical), others including *NCAM1*, *CPZ*, and *ARID3B* exhibited gene body hypermethylation

concordant with increased expression, aligning with canonical gene body regulation (Fig. 2D). To explore functional consequences of these epigenetically regulated genes, we performed pathway enrichment analysis using the PANTHER database. In both C/G$^+$ patient samples (Fig. 2E) and M07e cells (Fig. 2F), up-regulated DMGs were significantly enriched (false discovery rate $<$0.001, fold enrichment $>$2) in developmental and adhesion-related signaling pathways, including Wnt, TGF-β, cadherin, and integrin signaling, as well as angiogenesis and MAPK signaling cascades (Table S8). These pathways are tightly linked to leukemic cell plasticity, niche interactions, and immune escape.

Collectively, these results reveal that gene expression in C/G$^+$ leukemias is shaped by both canonical and non-canonical DNA methylation changes at promoters and gene bodies, converging on conserved developmental and adhesion programs. This layered epigenetic control may underlie the aggressive phenotype and lineage ambiguity observed in this high-risk leukemia subtype.

Differential methylation at CREs aligns with regulatory chromatin states and associates with gene expression changes

To examine the relationship between canonical and non-canonical DNA methylation and transcriptional regulation, we integrated histone modification data (H3K4me1, H3K4me3, H3K27me3, and H3K27ac) with a ChromHMM 10-state model (Table S9).[14,24] This model classified chromatin states into active enhancers, TSS-flanking regions, repressed transcription regions, and quiescent chromatin. Repressed (S2) and quiescent (E3) regions covered the majority of the genome (∼85%), while active promoter and enhancer states represented ∼17%, and bivalent or genic enhancers were rare (<1%) (Fig. 3A). Regions of these chromatin states contained significantly more hypermethylated CpGs compared with hypomethylated CpGs ($p < 0.05$), especially at promoters (Fig. 3C), whereas gene bodies and intergenic regions did not exhibit this trend.

We further evaluated the coincidence between differentially methylated chromatin states overlapped (≥50 bp) with accessible (primed) regions. The proportion of overlap varied across promoters, gene bodies, and intergenic regions (Fig. 3D and Table S10). Differentially methylated chromatin states in C/G$^+$ pAML, characterized by hypermethylation, frequently overlapped with open chromatin, particularly at the TSS—adjacent regions (TssFln and TssA). Conversely, hypomethylated, non-primed regions were predominantly associated with quiescent chromatin states (E3). Notably, a significant overlap was observed between primed chromatin and hypermethylated CpGs flanking TSS (E8 and E9), suggesting the presence of a hypermethylation-supported open-chromatin structure that could support transcriptional up-regulation through non-canonical epigenetic mechanisms.

We further analyzed the degree of correlation (Pearson's r) between DNA methylation changes at putative promoter-bound CpGs and expression of the corresponding genes across various chromatin states (E1—E10). The correlation between DNA methylation and gene expression was generally weak ($|r| < 0.2$) across states such as EnBiv (E1, $n = 63$), repressed polycomb (E2, $n = 890$), quiescent (E3, $n = 2852$), enhancer states (E4, $n = 559$; E5, $n = 755$; E6, $n = 1384$), TSS downstream regions (E7, $n = 923$), and EnhG (E10, $n = 231$). However, a relatively stronger negative correlation was observed between DNA methylation and expression at active TSS-proximal promoter states, including TssFln (E8, $n = 1450$; $r = -0.28$) and TssA (E9, $n = 470$; $r = -0.48$) (Fig. 4A). C/G-associated transcription factors like *ERG*, and CBFA2T3 partners like *GATA1* and *RUNX1T1* were found to be regulated within the EnhA2 (E5) state. Additionally, key C/G-restricted genes, including those with immunotherapeutic potential (*e.g.*, *CMTM5*, *DLX3*, *GP1BA*, *KIT*, *FRAS1*, *HPSE2*, and *KLRF2*), were identified in TSS-associated chromatin states (E7—E9) (Fig. 4A).[4,10,14,16,35] Further analysis underscored the dual role of DNA methylation in gene regulation, showing that both hypomethylated promoters (*e.g.*, *CMTM5* in Fig. 4B, and *GP1BA* in Fig. 4C) and hypermethylated promoters (*e.g.*, *HPSE2* in Fig. 4D, and *DLX3* in Fig. 4E) can support the up-regulation of genes. These modifications, regardless of their CpG island (CGI) context, were associated with accessible chromatin and enriched activating histone marks.

De novo chromatin looping aligns with differential DNA methylation in C/G pAML

To investigate the role of DNA methylation in genomic reorganization that confers a selective advantage for gene up-regulation, we analyzed differential promoter interactions between M07e and HSC. Using the CHICAGO pipeline (score > 5)[36], we identified significant chromatin loops. In M07e, we detected a substantial increase in the number of chromatin loops ($n = 35{,}008$, averaged over two replicates) (Fig. 5A), and an 80.7 kb reduction in the median linear distance between promoters and their interacting regions compared with HSC (Wilcoxon test, 95% CI, $p < 0.01$ (Fig. 5B). Notably, 61% of the differentially identified loops ($n = 62{,}044$) showed an increase in interaction strength (fold change $>$2), while 39% ($n = 39{,}098$) exhibited reduced interactions (Fig. 5C) in M07e cells. Given the importance of CTCF-mediated chromatin looping in genomic architecture, we assessed the coincidence of CTCF binding at these loops that originates from or are anchored to differentially methylated sites, focusing on both promoter-anchored and non-promoter interacting regions. We observed a higher number of CTCF-unbound, differentially methylated sites within the 5202 loops with increased interactions in M07e cells, including 3312 sites at promoter and 4040 at non-promoter regions (Fig. 5D). A similar trend was observed in 863 loops that exhibited decreased interactions (Fig. 5E).

Given the limitations of BeadChIP arrays in detecting strictly hyper- or hypomethylated DMRs, we analyzed loop-originating and loop-interacting regions containing hypermethylated, hypomethylated, a combination of both, or unmethylated CpGs. Notably, CTCF-bound loops with enhanced interactions in M07e cells ($n = 3052$) exhibited diverse CpG distributions: hypomethylated CpGs (23.3%), non-methylated CpGs (29.5%), and

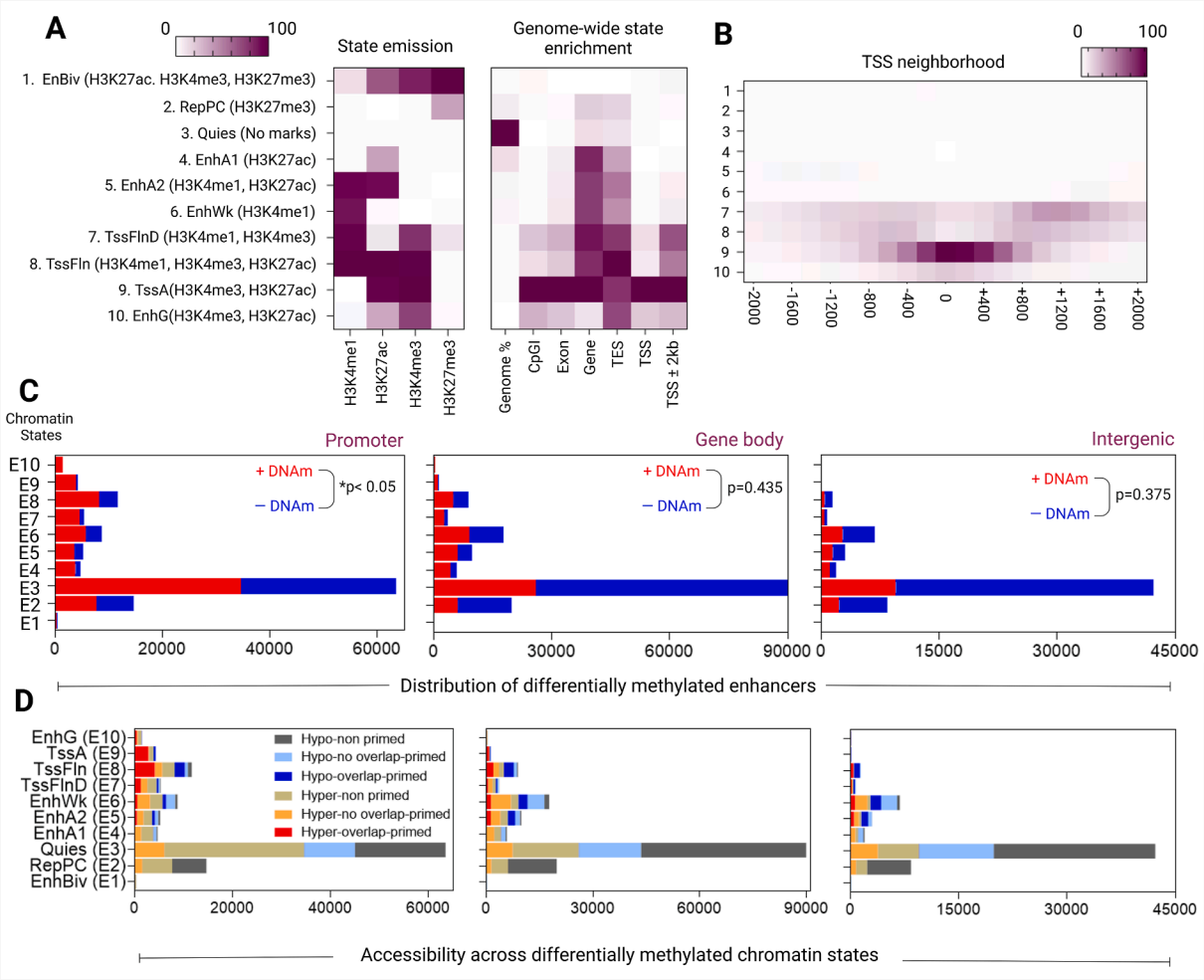

Figure 3 Chromatin state landscape and its association with DNA methylation in C/G$^+$ M07e cells. **(A)** The left panel displays a heatmap of emission parameters for the ten chromatin states, where each row represents a distinct chromatin state, and each column represents one of four histone modifications (H3K4me1, H3K4me3, H3K27ac, and H3K27me3) derived from chromatin immunoprecipitation-sequencing data in C/G$^+$ M07e cells (Thirant et al, 2017). The right panel shows a heatmap indicating the fold enrichment of each chromatin state across various external genomic annotations within M07e cells. **(B)** The heatmap illustrating the fold enrichment of each chromatin state across 200-bp bins spanning 2 kb around transcription start sites (TSSs), providing insight into chromatin state distribution in the proximity of gene promoters. **(C)** The stacked bar graphs presenting the proportion of chromatin states overlapping with hypermethylated and hypomethylated CpGs across promoters, gene bodies, and intergenic regions, highlighting the distinct methylation patterns associated with various chromatin states in these genomic regions. **(D)** The stacked bar charts showing the overlap proportions of differentially methylated chromatin states with open or closed chromatin states across promoters, gene bodies, and intergenic regions in M07e cells, providing a view of chromatin accessibility associated with differential methylation.

hypermethylated CpGs (31.5%) (Fig. 5D, E). To further elucidate the relationship between differential methylation and chromatin looping, we examined specific C/G-restricted genes (*e.g.*, *BMP2*, *MED12L*, *CMTM5*, and *KLRF2*), focusing on their associations with CTCF binding, H3K27ac-enriched histones, and differential methylation. For instance, in *BMP2* (Fig. 5F) and *MED12L* (Fig. 5G), both loop-originating and loop-interacting domains were anchored to CTCF-binding sites, coinciding with hypermethylated CpGs and enhancer-marked chromatin regions. In contrast, *CMTM5* (Fig. 5H) and *KLRF2* (Fig. 5I) exhibited loops lacking CTCF binding, with hypomethylated CpGs and enhancer-marked chromatin. These findings suggest that the interplay between CTCF binding and the methylation status of enhancer-marked chromatin distinctly shapes genomic architecture and modulates the transcriptional regulation of C/G-restricted genes.

C/G fusion leverages DNMT3B to induce an aberrant methylation landscape

Although the C/G fusion is a recognized oncogenic driver in C/G$^+$ pAML subtype, its precise role in shaping the aberrant DNA methylation landscape at CREs remains unclear. Prior studies suggest that C/G may bind to target sites through CBFA2T3, GLIS2, or a combination of both.[14] To investigate this, we performed CUT&RUN sequencing to examine

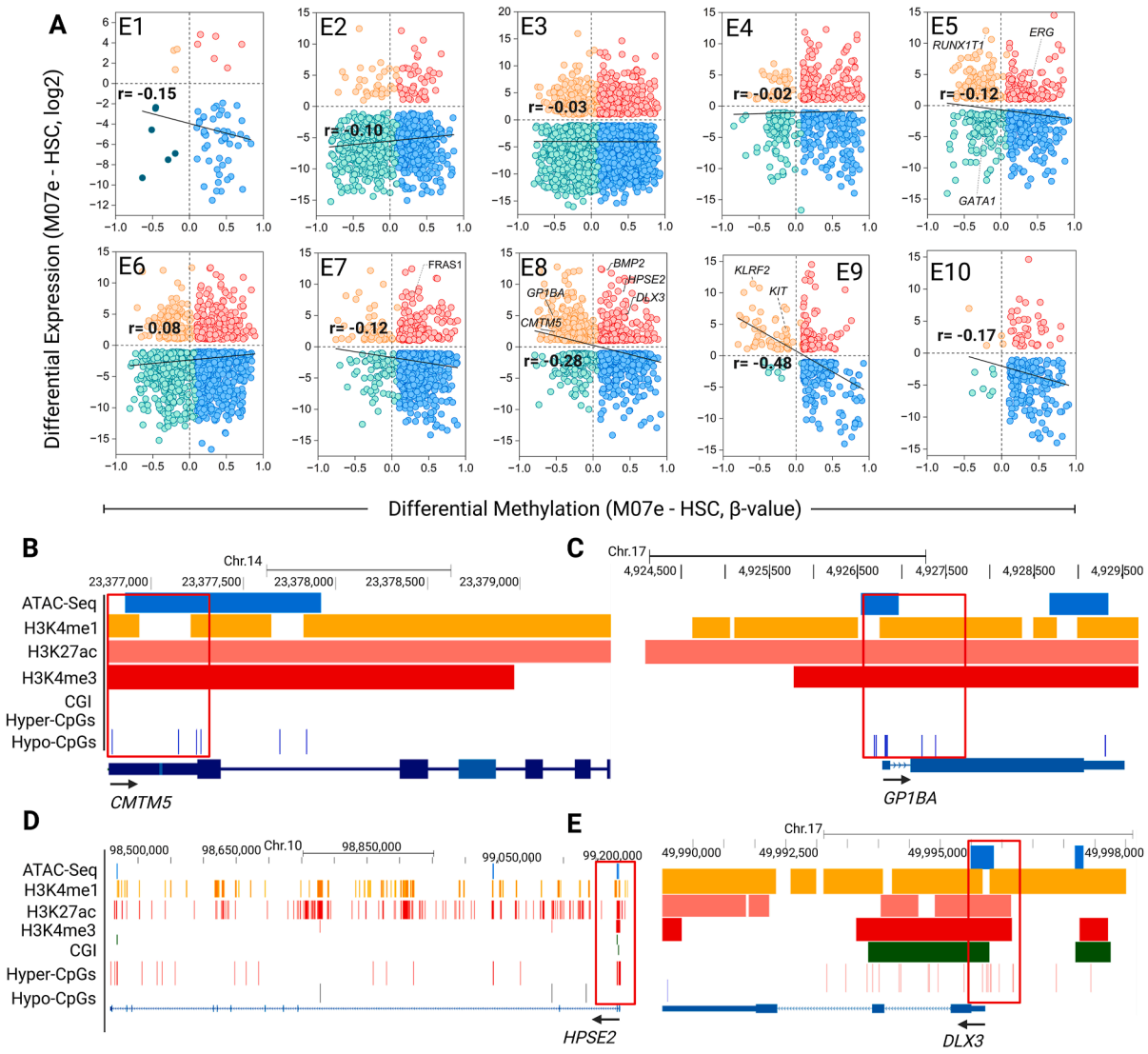

Figure 4 Correlation between DNA methylation, chromatin states, and gene expression in C/G^{+} M07e cells. **(A)** The scatter plots representing correlation (Pearson's *r*) between DNA methylation (average β-values) at gene promoters and the expression ($\log_2$ fold change) of the nearest genes across various chromatin states in M07e cell line. A significant negative correlation ($r > 0.2$) was observed between DNA methylation levels and gene expression for genes within regions flanking the transcription start site (TssFlnD; E8) and at active TSS regions (TssA; E9). This indicates that in these chromatin states, increased promoter methylation is associated with decreased gene expression. **(B–E)** Illustrations of the epigenetic landscapes of four representative C/G-restricted genes, showcasing contrasting methylation patterns and chromatin states at their promoters: (B) *CMTM5* and (C) *GP1BA* were up-regulated in C/G^{+} cells and exhibited hypomethylated CpGs at their promoters. These hypomethylated regions coincided with epigenetically primed chromatin, characterized by ATAC-sequencing peaks, indicative of open chromatin, and the presence of activating histone modifications (H3K4me1, H3K4me3, and H3K27ac). Conversely, (D) *HPSE2* and (E) *DLX3* were up-regulated despite containing hypermethylated CpGs at their promoters. These hypermethylated promoters also coincided with epigenetically primed chromatin and activating histone modifications, suggesting that up-regulation of these genes may be facilitated by chromatin accessibility and histone modifications rather than conventional methylation patterns.

genome-wide C/G occupancy in M07e and K562 cells (Fig. 6A). Our analysis showed lineage-specific binding distributions for CBFA2T3 and GLIS2^{Cent}, suggesting a disease-specific role of these proteins. We identified 6663 unique CBFA2T3 peaks in M07e cells and 2894 in K562 cells, with only 9.3% overlap ($n = 986$) between the two cell lines. Similarly, 2327 unique GLIS2^{Cent} peaks were identified in M07e cells and 4836 in K562 cells, with 1.6% overlap ($n = 118$). Further analysis in M07e cells revealed that 1852 of the 7649 CBFA2T3-bound peaks, 350 of the 2445 GLIS2^{Cent}-bound peaks, and 518 of the 1902 co-bound peaks coincided with DMCs (Fig. 6B). Notably, a significant proportion of these peaks contained hypomethylated CpGs (63.9% for CBFA2T3, 72% for GLIS2^{Cent}, and 72.7% for co-bound peaks). This hypomethylation pattern contrasts with the hyper-methylated landscape observed across the genome in C/G^{+}

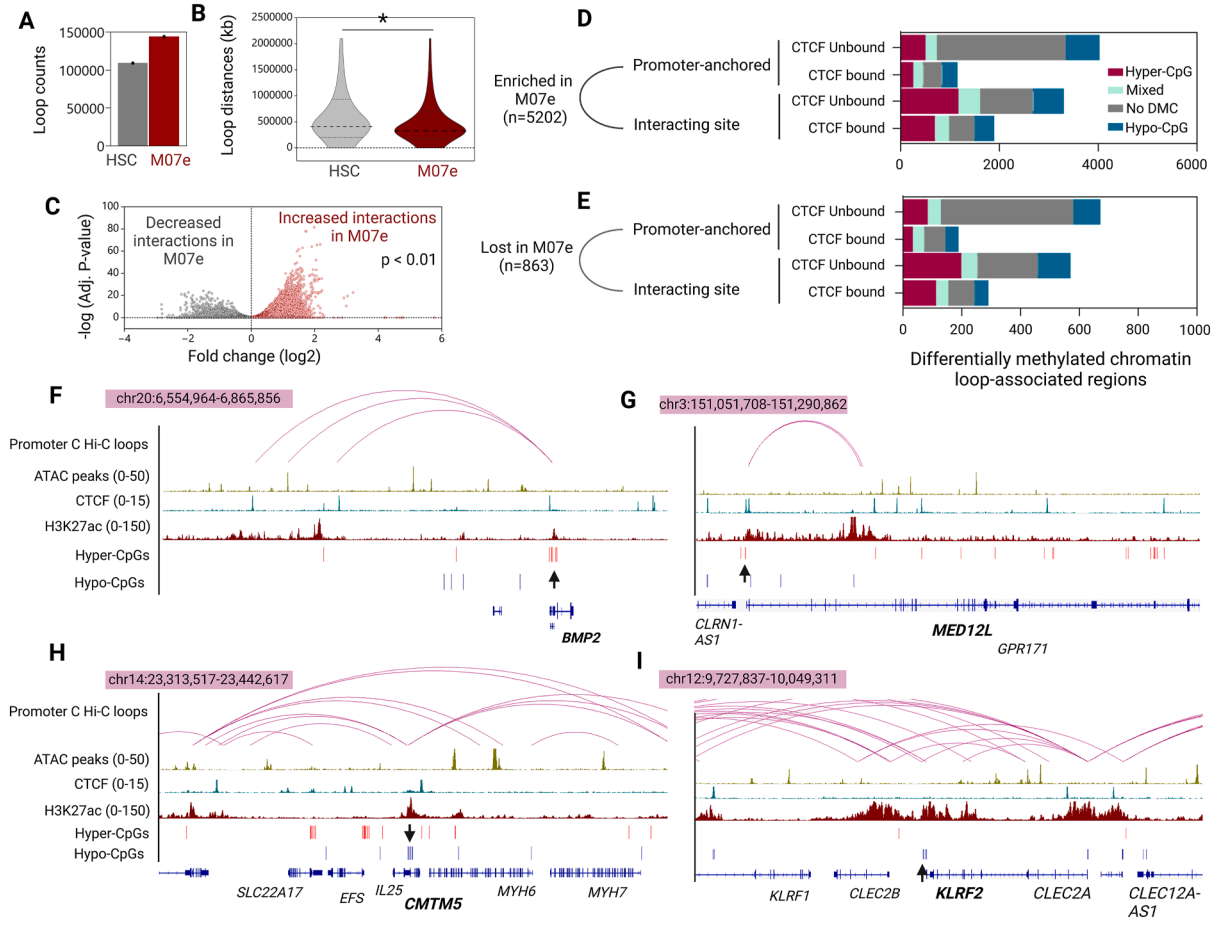

Figure 5 Promoter-interacting chromatin loops and their association with DNA methylation in C/G$^+$ M07e cells. **(A)** Promoter capture chromosome conformation capture (PCHi-C) analysis shows the number of promoter-interacting loops in M07e cells compared with CD34$^+$ hematopoietic stem cells (HSC). **(B)** The violin plot representing the median distance between promoter origins and interacting regions within chromatin loops in M07e cells versus HSC. **(C)** The scatter plot highlighting the differentially enriched loops in M07e cells relative to HSC. **(D, E)** The stacked bar graphs showing the proportions of CTCF binding at hyper- or hypo-methylated CpGs within promoter-anchored and non-promoter interacting regions that are either differentially enriched (D) or absent (E) in M07e compared with HSC. **(F–I)** Integrative Genomics Viewer (IGV) representations of two genes, (F) *BMP2* and (G) *MED12L*, demonstrate hypermethylated promoters with coincident CTCF binding, H3K27ac enrichment, and promoter-anchored loops, suggesting a role for enhancer-bound hypermethylated CpGs in chromatin remodeling. Conversely, chromatin looping associated with hypomethylation was observed at the promoters of (H) *CMTM5* and (I) *KLRF2*.

pAML, suggesting further investigation into potential relationships between C/G fusion and key epigenetic regulators.

Among the major epigenetic regulators differentially expressed (log fold change >1) in C/G$^+$ pAML patients (n = 24) compared with NBM isolates (n = 10), CBFA2T3 expression exhibited a significant negative correlation with histone deacetylase 4 (HDAC4) in NBM (Spearman's $\rho = -0.76$, with $\rho > 0.4$ and $p < 0.05$ considered significant), though this correlation was weaker in C/G$^+$ patients ($\rho = -0.11$). In contrast, GLIS2 showed minimal correlation with other epigenetic regulators. Notably, in C/G$^+$ pAML, both CBFA2T3 and GLIS2 were significantly positively correlated with DNMT3B ($\rho = 0.74$) and HDAC5 ($\rho = 0.49$) (Fig. 6C). These findings support the hypothesis that the C/G fusion may enhance DNMT3B expression and activity, potentially driving genome-wide aberrant *de novo* hypermethylation in C/G$^+$ pAML.

To test this hypothesis, we performed CUT&RUN profiling of two activating histone modifications—H3K4me3 and H3K27ac—and integrated these data with CBFA2T3 and GLIS2^{Cent} binding profiles. The *DNMT3B* promoter was marked by H3K4me3 in both M07e and K562 cell lines (Fig. 6D, E), however, co-occupancy of CBFA2T3 and GLIS2^{Cent} was observed exclusively in M07e cells, consistent with direct targeting by the C/G fusion (Fig. 6D). The specificity of C/G fusion binding was further supported by the presence of a GLIS2 binding peak detected only with the antibody targeting the central domain of GLIS2 and not with the N-terminal-specific GLIS2 antibody (Fig. 6D). Additionally, we observed enrichment of H3K27ac near exon-2, the translation initiation site of *DNMT3B* in M07e cells but not in K562 cells.[37] Although K562 is not of myeloid lineage, it was selected for comparison based on its relatively high and comparable expression of *CBFA2T3*, *GLIS2*, and *DNMT3B*, as confirmed by RNA-sequencing TPM values

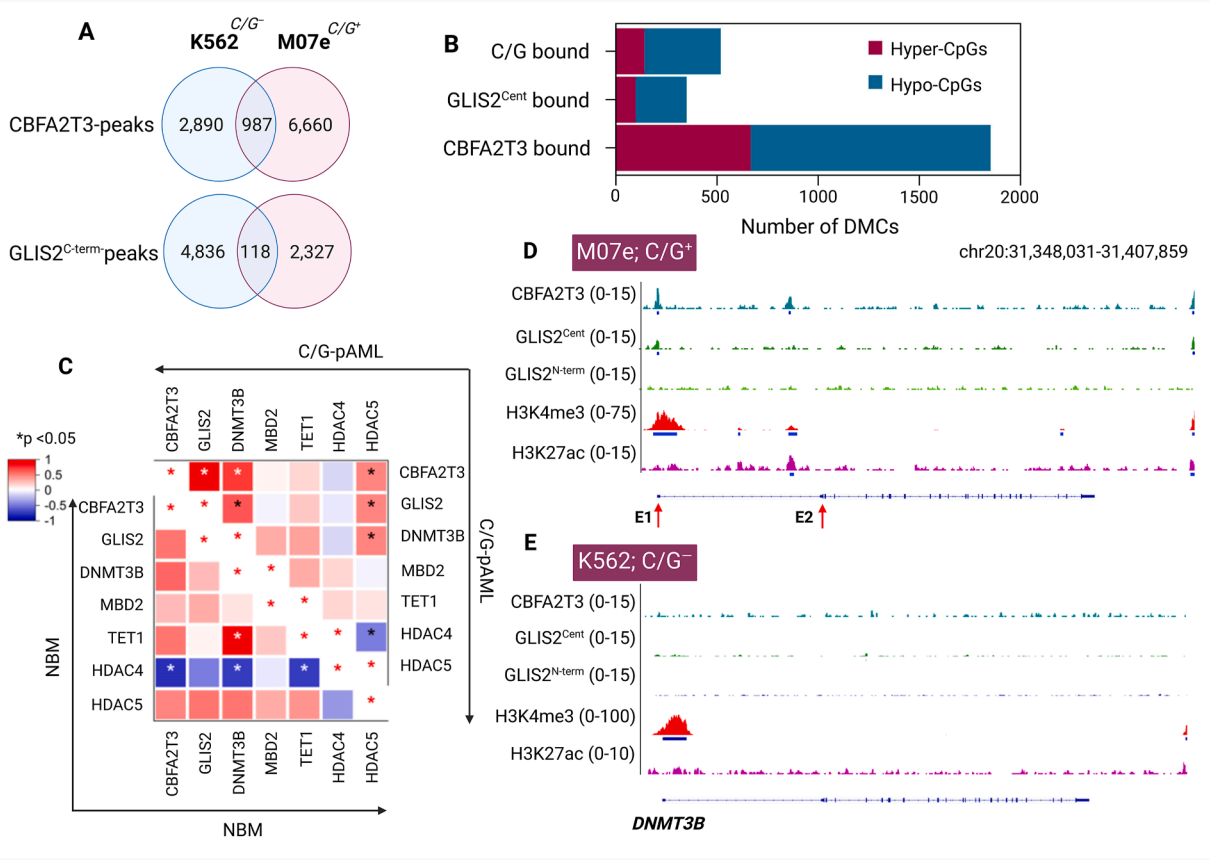

Figure 6 CBFA2T3-GLIS2 binding and its association with DNA methylation and gene regulation. **(A)** The Venn diagrams displaying the distribution of unique and shared CBFA2T3 and GLIS2 binding peaks between M07e and K562 cells, as identified through CUT&RUN sequencing. **(B)** The stacked bar graph showing the proportion of CBFA2T3, GLIS2, or combined CBFA2T3-GLIS2 (C/G) binding peaks overlapping with hyper- and hypomethylated CpGs in M07e cells. **(C)** Spearman rank correlation matrices for differentially expressed genes (log fold change >1, $p < 0.05$) in C/G$^+$ pediatric acute myeloid leukemia (AML) patients ($n = 24$) compared with normal bone marrow (NBM) ($n = 10$), specifically encoding epigenetic regulatory proteins. Correlations with Spearman's coefficient $\rho > 0.4$ and $p < 0.05$ were considered significant. A significant negative correlation (blue) was observed between CBFA2T3 and HDAC4 in NBM isolates, but this correlation was weaker in C/G$^+$ pediatric AML. In contrast, positive correlations (red) were observed between CBFA2T3/GLIS2 and HDAC5/DNMT3B expression in C/G$^+$ pediatric AML compared with NBM isolates. **(D, E)** CUT&RUN sequencing confirmed the specific binding of both CBFA2T3 and GLIS2 proximal to the promoter and exon-2 (translation start site) of *DNMT3B* in M07e cells (D), but this binding was absent in K562 cells (E).

retrieved from the Expression Atlas (Fig. S5). These characteristics allowed us to control for gene dosage effects while isolating fusion-specific binding patterns. In contrast, other AML-derived cell lines used elsewhere in this study (*e.g.*, KG1A, KASUMI-1, ME-1) do not confer additional interpretive advantage in this setting, as they lack expression parity and may introduce confounding lineage-specific regulatory differences. Together, these findings support a model in which the C/G fusion directly engages the *DNMT3B* promoter to drive its transcriptional up-regulation, enabling aberrant methylation of CREs and reinforcement of the leukemic gene expression program in C/G$^+$ AMKL.

Loss of DNMT3B reshapes the DNA methylation and transcriptional programs

To investigate the role of *DNMT3B* in regulating DNA methylation and transcription, we generated *DNMT3B* KO M07e cells using CRISPR-Cas9-mediated genome editing. A sgRNA targeting exon 6 of *DNMT3B* was cloned into a lentiviral vector for delivery (Fig. 7A). Western blotting analysis confirmed complete loss of DNMT3B protein in KO cells compared with WT and scramble controls, with β-actin as a loading control (Fig. 7B). Genome-wide DNA methylation profiling via RRBS identified 3670 DMRs in KO cells, comprising 2475 hypermethylated and 1195 hypomethylated regions. Notably, DNMT3B loss resulted in DNA methylation changes across 1290 enhancer-bound and 1185 non-enhancer-bound DMRs, with 612 enhancer-bound and 583 non-enhancer-bound regions exhibiting decreased DNA methylation (Fig. 7C). Further analysis revealed that both hypermethylated and hypomethylated DMRs were significantly enriched at promoters compared with gene bodies ($p < 0.05$, two-tailed *t*-test) (Fig. 7D). Kyoto Encyclopedia of Genes and Genomes (KEGG) pathway enrichment analysis of DMR-associated genes highlighted significant enrichment in cellular adhesion pathways (Fig. 7E and

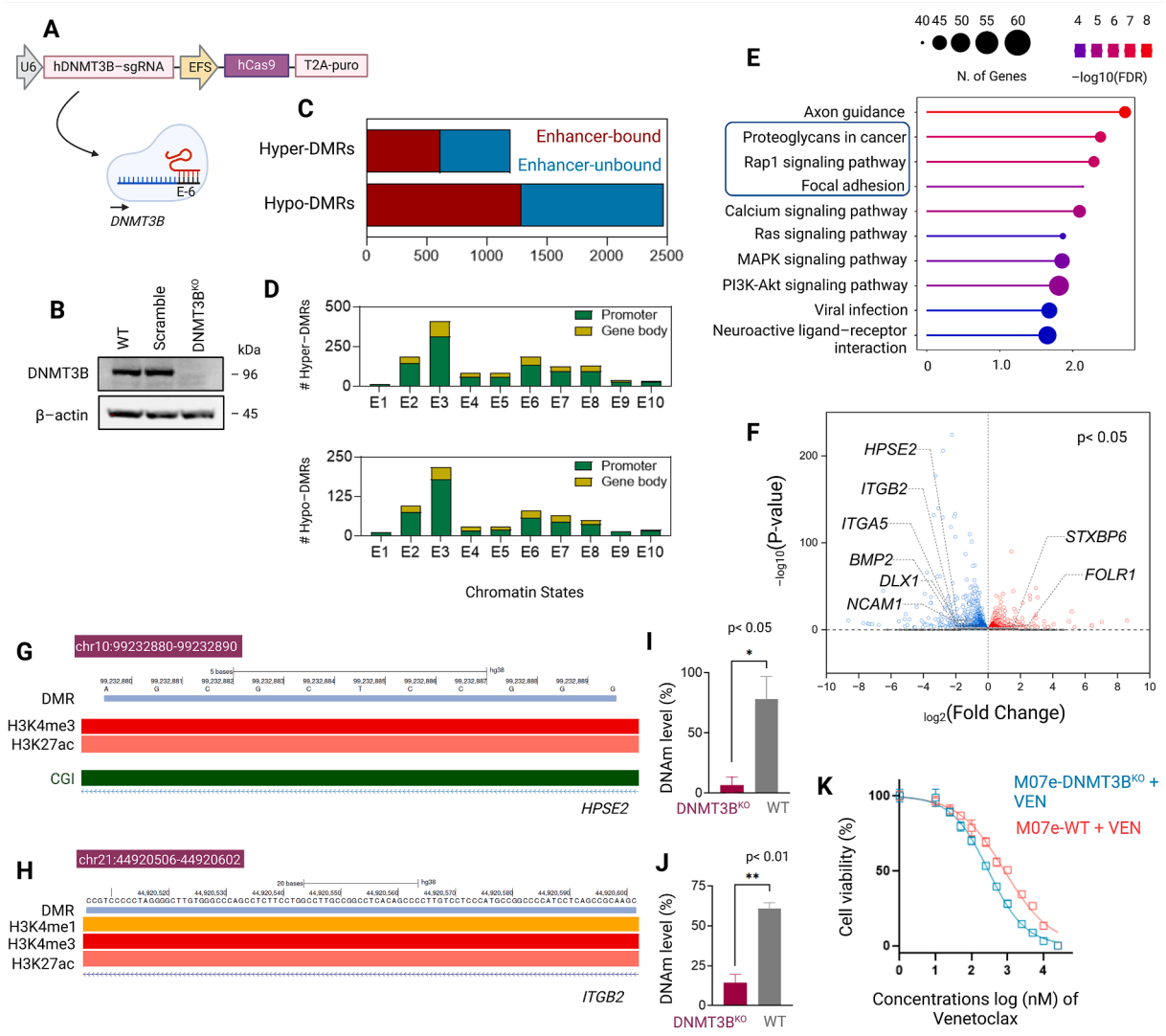

Figure 7 Functional impact of DNMT3B knockout on DNA methylation, gene expression, and drug sensitivity in M07e cells. **(A)** Schematic representation of the CRISPR-Cas9-mediated knockout of DNMT3B (*DNMT3B* KO) in M07e cells. The U6 promoter drives expression of an *hDNMT3B*-targeting single-guide RNA (sgRNA), while an EFS promoter controls Cas9 expression along with a T2A-linked puromycin resistance cassette for selection. **(B)** Western blotting analysis confirmed DNMT3B depletion in *DNMT3B*KO cells. Wild-type (WT) and scramble control cells served as references. β-actin was used as a loading control. **(C)** Distribution of differentially methylated regions (DMRs) following *DNMT3B* KO, categorized as hypermethylated (Hyper-DMRs) or hypomethylated (Hypo-DMRs). DMRs were further classified based on their localization within enhancer-bound (red) or enhancer-unbound (blue) regions. **(D)** Annotation of Hyper-DMRs (top) and Hypo-DMRs (bottom) across chromatin states (E1—E10) in M07e cells. The distribution of DMRs in promoters (yellow) was significantly higher than in gene bodies (green) (two-tailed *t*-test, $p < 0.05$), highlighting preferential methylation changes in regulatory regions. **(E)** Kyoto Encyclopedia of Genes and Genomes (KEGG) pathway enrichment analysis of genes associated with DMRs, showing significant enrichment in signaling pathways, including axon guidance, focal adhesion, MAPK signaling, and PI3K-Akt signaling. Circle size represents the number of genes in each pathway, and color intensity corresponds to statistical significance ($-\log_{10}$ false discovery rate). **(F)** The volcano plot displaying differentially expressed genes in *DNMT3B* KO versus WT cells. Key genes with significant changes ($p < 0.05$) are labeled, including *HPSE2*, *ITGB2*, *ITGA5*, *BMP2*, *DLX1*, *NCAM1*, *STXBP6*, and *FOLR1*. The red and blue indicate up-regulated and down-regulated genes, respectively. **(G, H)** Genome browser tracks of representative Hypo-DMRs at *HPSE2* (G) and *ITGB2* (H) loci. Tracks show the presence of active histone modifications (H3K4me3, H3K27ac) and CpG islands (CGI). Loss of DNA methylation at these loci correlates with active chromatin features. **(I, J)** Quantification of DNA methylation levels at *HPSE2* (I) and *ITGB2* (J) loci in WT and *DNMT3B* KO cells. DNA methylation levels were significantly reduced in *DNMT3B* KO cells ($p < 0.05$ and $p < 0.01$, respectively). **(K)** Cell viability assay assessed the sensitivity of WT and *DNMT3B*KO M07e cells to venetoclax (VEN) treatment. *DNMT3B* KO cells exhibited increased sensitivity to VEN, indicating a potential epigenetic mechanism affecting drug response.

Table S11), suggesting a role for DNMT3B in epigenetic regulation of adhesion-related mechanisms.

RNA sequencing of *DNMT3B* KO cells identified 4286 differentially expressed genes, including 1030 up-regulated and 1730 down-regulated genes (false discovery rate <0.05; $\log_2$ fold change cutoff). Among these, key adhesion-associated genes (*e.g.*, *HPSE2*, *ITGB2*, *ITGA5*, *BMP2*, *DLX1*, and *NCAM1*) were significantly down-regulated (Fig. 7F), indicating DNMT3B's role in promoting adhesion-related gene expression in C/G$^+$ pAML. Integrated analysis of RNA sequencing and DNA methylation profiling revealed that 346 differentially expressed genes were directly associated with DMRs, confirming a coordinated regulatory mechanism (Fig. S4). To validate these findings, we examined DNA methylation levels at the *HPSE2* and *ITGB2* loci. *HPSE2* exhibited significant hypomethylation, with a 71% reduction across five CpGs spanning 12 bp ($p < 0.05$) (Fig. 7G–I), while *ITGB2* showed a 36% reduction across five CpGs spanning 97 bp ($p < 0.05$) (Fig. 7H–J), supporting DNMT3B-dependent regulation of adhesion-associated genes.

To assess whether DNMT3B loss influences baseline cellular fitness, we first compared the viability of WT and DNMT3B KO M07e cells under standard culture conditions. DNMT3B KO cells exhibited a modest but statistically significant reduction in viability (~14%, $p < 0.05$) relative to WT cells (Fig. S6). Given this modest effect, we next tested whether DNMT3B ablation could sensitize C/G$^+$ pAML cells to chemotherapy. Because C/G$^+$ leukemias are typically resistant to BCL2 inhibition,[38] we evaluated the response of WT and DNMT3B KO cells to venetoclax. WT M07e cells were relatively resistant ($IC_{50} = 0.82$ μM), whereas DNMT3B KO cells showed markedly enhanced sensitivity, with an IC_{50} reduced to 0.29 μM (Fig. 7K). These results indicate that loss of DNMT3B may partially overcome intrinsic venetoclax resistance in C/G$^+$ pAML, highlighting a potential therapeutic vulnerability. To determine whether DNMT3B loss affects apoptotic susceptibility, we performed annexin V/PI staining in DNMT3B KO M07e cells treated with or without venetoclax. Under basal conditions, DNMT3B KO cells were largely viable (~85%), with minimal apoptosis, indicating that DNMT3B depletion alone does not induce cell death. Venetoclax treatment significantly reduced viability (~50%) and markedly increased late apoptotic (~13%–~60%) and necrotic (~1%–~45%) populations, while early apoptosis remained unchanged (Fig. S7). These findings suggest that DNMT3B loss enhances apoptotic progression in response to BCL2 inhibition, possibly by priming mitochondrial-mediated cell death pathways.

Discussion

Our integrative multi-omics study reveals distinct epigenetic features in C/G$^+$ pAML, providing insights into transcriptional reprogramming driven by DNA methylation alterations and enhancer dynamics. DNA methylome analysis of C/G$^+$ pAML patient samples encompassing both M7 and non-M7 lineages, along with representative cell lines, reveals that C/G-specific DMCs are predominantly hypermethylated across promoters, gene bodies, and intergenic regions (Fig. 1E–G). Differences in DMC distribution between patient samples and cell lines may stem from the fact that most patient samples were derived from newly diagnosed cases, whereas cell lines may have acquired additional genetic and epigenetic modifications over time. Despite this, the presence of the C/G fusion consistently led to the close clustering of patient-derived blasts or cell lines with respect to control samples.

Interestingly, although promoter hypermethylation is traditionally associated with transcriptional repression via transcription factor-binding inhibition and chromatin condensation, 46.7% (498/1062) of up-regulated differentially expressed genes in C/G$^+$ patients exhibited hypermethylated CpGs at their promoters (Fig. 2C). This atypical hypermethylation pattern, previously observed in *de novo* (non-Down syndrome) AMKL cases,[19,39,40] deviates from canonical cancer methylation profiles, possibly reflecting enhancer-mediated activation driven by chromatin modifications.[41] These findings prompted further exploration of DMC overlap with chromatin states defined by histone modifications, revealing that hypermethylated CpGs in promoter regions frequently overlapped with varied chromatin states, in contrast to hypomethylated CpGs (Fig. 3C).

Furthermore, clusters of up-regulated genes with hypermethylated promoter CpGs were associated with distinct chromatin states (Fig. 4A). For instance, ERG up-regulation and GATA1 down-regulation—hallmark events in C/G$^+$ pAML—were both associated with non-canonical DNA methylation patterns at their promoters in the E5 chromatin state. Similarly, genes identified as potential immunotherapy targets, such as *FRAS1* and *HPSE2*,[35] exhibited promoter hypermethylation despite being up-regulated, likely through association with the enhancer-chromatin states (E7 and E8). Notably, these DMC-linked chromatin states exhibited limited overlap (≥50 bp) with open or "primed" chromatin states. The lack of concordance between chromatin accessibility and gene expression changes, as previously noted in other studies,[42,43] suggests either a context-dependent role for activating transcription factors or an instance of atypical chromatin remodeling. To further elucidate the impact of promoter DNA methylation on chromatin architecture in the C/G$^+$ genome, we conducted PCHi-C analysis, which revealed that while CTCF-bound loops predominantly overlapped with non-methylated or hypomethylated CpGs, hypermethylated CpGs were often enriched within enhancer-marked chromatin and involved in *de novo* chromatin looping. These findings indicate that hypermethylated CpGs may contribute to the up-regulation of genes critical for sustaining the leukemic transcriptional program in C/G$^+$ pAML through non-canonical chromatin remodeling mechanisms (Fig. 5).

Our analysis also highlighted minimal shared binding peaks of CBFA2T3/GLIS2^{Cent} between C/G$^+$ M07e cells and C/G$^-$ K562 cells (Fig. 6A), suggesting that C/G fusion partners exhibit unique binding profiles and context-dependent functional roles. While the C/G fusion is a key driver of this leukemia subtype, its exact mechanism in establishing aberrant DNA methylation patterns remains unclear, particularly since common epigenetic modifiers frequently mutated in adult AML (*e.g.*, *IDH1*, *IDH2*, *TET2*, or *DNMT3A*) are not mutated in C/G$^+$ pAML.[44] This implies a distinctive mechanism underlying C/G-driven hypermethylation. Our study also found a negative correlation of

CBFA2T3/GLIS2 expression with *HDAC4*, but a positive correlation with *HDAC5*, consistent with prior findings of *HDAC5* overexpression and *HDAC4* down-regulation in AML and other hematological malignancies.[36,45,46] Although the simultaneous presence of HDAC5 overexpression and genome-wide H3K27ac enrichment in the C/G genome may seem contradictory, past studies have shown no consistent link between HDAC activity and H3K27ac levels.[47,48] The observed genome-wide hypermethylation is instead likely attributed to the positive correlation between CBFA2T3/GLIS2 and *DNMT3B* expression. This is further supported by C/G fusion binding near the TSS and the first exon of *DNMT3B* in M07e but not in K562 cells (Fig. 6D, E).

To investigate the functional impact of DNA methylation alterations, we generated *DNMT3B* KO M07e cells, given the strong correlation between *DNMT3B* expression and C/G-driven methylation. Loss of *DNMT3B* led to widespread hypomethylation, particularly within enhancer-associated regions (Fig. 7C), reinforcing the role of *DNMT3B*-mediated methylation in enhancer regulation. Interestingly, hypomethylation events were significantly more enriched at promoter regions compared with gene bodies (two-tailed *t*-test, $p < 0.05$) (Fig. 7D), indicating preferential epigenetic deregulation of regulatory elements.

Furthermore, DNMT3B KO cells exhibited increased sensitivity to venetoclax compared with WT cells (Fig. 7K), suggesting that DNA methylation contributes to apoptotic resistance in C/G$^+$ pAML. Apoptosis profiling revealed a marked shift from viability to late apoptotic and necrotic states following venetoclax treatment (Fig. S7), suggesting that DNMT3B loss primes leukemic cells for apoptotic execution upon BCL2 inhibition. While the precise molecular mediators of this effect remain to be defined, these findings highlight the broader role of DNMT3B in modulating therapeutic response. Given the urgent need for effective treatments for C/G$^+$ pAML, particularly in the absence of targeted therapies, identifying downstream effectors of DNMT3B remains a priority. Although DNMT3B has previously been implicated in AML, our data position it within a distinct C/G-driven enhancer regulatory axis. Moreover, our integrative analysis identified several DNMT3B-regulated genes (*e.g.*, *HPSE2*, *ITGB2*, *DLX1*, *BMP2*, *NCAM1*) involved in adhesion signaling, and immune regulation.[10,35] While not functionally validated here, these targets represent promising candidates for future mechanistic and translational studies.

Prior studies have shown that C/G exhibits a restricted genome-wide binding profile, occupying fewer than 2000 loci, with only ~20% of its target genes showing differential expression.[14] This suggests that C/G exerts its oncogenic effects primarily through downstream regulatory networks rather than direct transcriptional activation. One such critical effector is DNMT3B, whose expression is driven by direct C/G binding at its promoter, leading to widespread aberrant DNA methylation. This mechanism parallels the function of overexpressed ERG, which cooperates with C/G to establish *de novo* SEs, reinforcing a transcriptional feedforward loop that amplifies oncogenic gene expression, including *KIT*.[16]

Collectively, our findings reveal that promoter hypermethylation in C/G$^+$ pAML frequently coincides with enhancer chromatin elements, explaining the up-regulation of C/G-specific genes. Disrupting these transcriptional and epigenetic circuits could serve as a viable therapeutic strategy in C/G$^+$ pAML, with implications that may extend beyond C/G$^+$ pAML to other fusion-driven cancers, where similar oncogenic processes operate.[49–52]

CRediT authorship contribution statement

Samrat Roy Choudhury: Writing – review & editing, Writing – original draft, Supervision, Methodology, Investigation, Funding acquisition, Formal analysis, Data curation, Conceptualization. **Akhilesh Kaushal:** Writing – original draft, Software, Formal analysis, Data curation. **Pritam Biswas:** Writing – original draft, Methodology, Formal analysis. **Cory Padilla:** Writing – original draft, Methodology, Formal analysis. **Jay F. Sarthy:** Writing – original draft, Methodology, Formal analysis. **Arundhati Chavan:** Writing – original draft, Methodology. **Giselle Almeida Gonzalez:** Writing – original draft, Methodology. **Soheil Meshinchi:** Writing – original draft, Formal analysis. **Jason E. Farrar:** Writing – original draft, Resources, Formal analysis.

Ethics declaration

DNA methylation arrays were performed on specimens from consented patients enrolled in the TARGET-AML study (phs000465). The data are accessible through the Database of Genotypes and Phenotypes (dbGaP) and the NCI Genomic Data Commons (GDC). This study analyzed genomic data from these publicly available datasets and did not involve the enrollment of human subjects specifically for this research.

Conflict of interests

The authors declared no competing interests.

Funding

This study is supported by the US Department of Defense RCRP Program (No. HT9425-24-1-0932), the National Institute of General Medical Sciences (USA) (No. 2P20GM121293), and the Marion B. Lyon New Scientist Development Award of Arkansas Children's Research Institute (USA) (No. LYON5069, awarded to S.R.C.). Partial support is also provided by start-up funds from the University of Arkansas for Medical Sciences and Arkansas Bioscience Institute (USA) (No. ABIRC4426 to S.R.C.).

Appendix A. Supplementary data

Supplementary data to this article can be found online at https://doi.org/10.1016/j.gendis.2025.101843.

References

1. Lowenberg B, Downing JR, Burnett A. Acute myeloid leukemia. *N Engl J Med*. 1999;341(14):1051–1062.
2. Döhner H, Weisdorf DJ, Bloomfield CD. Acute myeloid leukemia. *N Engl J Med*. 2015;373(12):1136–1152.

3. Quinlan AR, Hall IM. BEDTools: a flexible suite of utilities for comparing genomic features. *Bioinformatics*. 2010;26(6):841—842.
4. Gruber TA, Larson Gedman A, Zhang J, et al. An Inv(16)(p13.3q24.3)-encoded CBFA2T3-GLIS2 fusion protein defines an aggressive subtype of pediatric acute megakaryoblastic leukemia. *Cancer Cell*. 2012;22(5):683—697.
5. Pagano L, Pulsoni A, Vignetti M, et al. Acute megakaryoblastic leukemia: experience of GIMEMA trials. *Leukemia*. 2002;16(9):1622—1626.
6. Gruber TA, Downing JR. The biology of pediatric acute megakaryoblastic leukemia. *Blood*. 2015;126(8):943—949.
7. Lopez CK, Malinge S, Gaudry M, Bernard OA, Mercher T. Pediatric acute megakaryoblastic leukemia: multitasking fusion proteins and oncogenic cooperations. *Trends Cancer*. 2017;3(9):631—642.
8. Eidenschink Brodersen L, Alonzo TA, Menssen AJ, et al. A recurrent immunophenotype at diagnosis independently identifies high-risk pediatric acute myeloid leukemia: a report from children's oncology group. *Leukemia*. 2016;30(10):2077—2080.
9. Matos R, Ferreira G, Costa E, et al. Clinical and molecular report of a rare RAM positive non-down syndrome infant CBFA2T3-GLIS2 negative, presenting the driver P210-BCR-ABL1. *Hematol Transfus Cell Ther*. 2022;44:S344—S345.
10. Smith JL, Ries RE, Hylkema T, et al. Comprehensive transcriptome profiling of cryptic *CBFA2T3-GLIS2* fusion-positive AML defines novel therapeutic options: a COG and TARGET pediatric AML atudy. *Clin Cancer Res*. 2020;26(3):726—737.
11. de Rooij JD, Branstetter C, Ma J, et al. Pediatric non-down syndrome acute megakaryoblastic leukemia is characterized by distinct genomic subsets with varying outcomes. *Nat Genet*. 2017;49(3):451—456.
12. Hara Y, Shiba N, Ohki K, et al. Prognostic impact of specific molecular profiles in pediatric acute megakaryoblastic leukemia in non-down syndrome. *Genes Chromosomes Cancer*. 2017;56(5):394—404.
13. Thiollier C, Lopez CK, Gerby B, et al. Characterization of novel genomic alterations and therapeutic approaches using acute megakaryoblastic leukemia xenograft models. *J Exp Med*. 2012;209(11):2017—2031.
14. Thirant C, Ignacimouttou C, Lopez CK, et al. ETO2-GLIS2 hijacks transcriptional complexes to drive cellular identity and self-renewal in pediatric acute megakaryoblastic leukemia. *Cancer Cell*. 2017;31(3):452—465.
15. Thirant C, Lopez C, Malinge S, Mercher T. Molecular pathways driven by ETO2-GLIS2 in aggressive pediatric leukemia. *Mol Cell Oncol*. 2017;4(6):e1345351.
16. Benbarche S, Lopez CK, Salataj E, et al. Screening of ETO2-GLIS2-induced super Enhancers identifies targetable cooperative dependencies in acute megakaryoblastic leukemia. *Sci Adv*. 2022;8(6):eabg9455.
17. Tijssen MR, Cvejic A, Joshi A, et al. Genome-wide analysis of simultaneous GATA1/2, RUNX1, FLI1, and SCL binding in megakaryocytes identifies hematopoietic regulators. *Dev Cell*. 2011;20(5):597—609.
18. Masetti R, Bertuccio SN, Astolfi A, et al. Hh/Gli antagonist in acute myeloid leukemia with CBFA2T3-GLIS2 fusion gene. *J Hematol Oncol*. 2017;10(1):26.
19. Kaushal A, Biswas P, Farrar J, Choudhury SR. Abstract P16: CBFA2T3-GLIS2 fusion leads to a distinct DNA methylation enhancer landscape in pediatric acute myeloid leukemia. *Blood Cancer Discov*. 2024;5(2_Supplement):P16. P16.
20. Challen GA, Sun D, Mayle A, et al. Dnmt3a and Dnmt3b have overlapping and distinct functions in hematopoietic stem cells. *Cell Stem Cell*. 2014;15(3):350—364.
21. Rinaldi L, Datta D, Serrat J, et al. Dnmt3a and Dnmt3b associate with enhancers to regulate human epidermal stem cell homeostasis. *Cell Stem Cell*. 2016;19(4):491—501.
22. Choudhury SR, Ashby C, Tytarenko R, et al. The functional epigenetic landscape of aberrant gene expression in molecular subgroups of newly diagnosed multiple myeloma. *J Hematol Oncol*. 2020;13(1):108.
23. Choudhury SR, Walker BA. A rapid and robust protocol for reduced representation bisulfite sequencing in multiple myeloma. *Methods Mol Biol*. 2018;1792:179—191.
24. Ernst J, Kellis M. Chromatin-state discovery and genome annotation with ChromHMM. *Nat Protoc*. 2017;12(12):2478—2492.
25. Ernst J, Kellis M. Large-scale imputation of epigenomic datasets for systematic annotation of diverse human tissues. *Nat Biotechnol*. 2015;33(4):364—376.
26. Robinson JT, Thorvaldsdóttir H, Winckler W, et al. Integrative genomics viewer. *Nat Biotechnol*. 2011;29(1):24—26.
27. Zhang Y, Liu T, Meyer CA, et al. Model-based analysis of ChIP-Seq (MACS). *Genome Biol*. 2008;9(9):R137.
28. Schoenfelder S, Javierre BM, Furlan-Magaril M, Wingett SW, Fraser P. Promoter capture Hi-C: high-resolution, genome-wide profiling of promoter interactions. *J Vis Exp*. 2018;136:e57320.
29. Skene PJ, Henikoff S. An efficient targeted nuclease strategy for high-resolution mapping of DNA binding sites. *eLife*. 2017;6:e21856.
30. Meers MP, Tenenbaum D, Henikoff S. Peak calling by sparse enrichment analysis for CUT&RUN chromatin profiling. *Epigenetics Chromatin*. 2019;12(1):42.
31. Bae S, Park J, Kim JS. Cas-OFFinder: a fast and versatile algorithm that searches for potential off-target sites of Cas9 RNA-guided endonucleases. *Bioinformatics*. 2014;30(10):1473—1475.
32. Park J, Bae S, Kim JS. Cas-designer: a web-based tool for choice of CRISPR-Cas9 target sites. *Bioinformatics*. 2015;31(24):4014—4016.
33. Frett B, Stephens KE, Koss B, et al. Enhancer-activated RET confers protection against oxidative stress to KMT2A-rearranged acute myeloid leukemia. *Cancer Sci*. 2024;115(3):963—973.
34. Roy Choudhury S, Heflin B, Taylor E, Koss B, Avaritt NL, Tackett AJ. CRISPR/dCas9-KRAB-mediated suppression of S100b restores p53-mediated apoptosis in melanoma cells. *Cells*. 2023;12(5):730.
35. Le Q, Hadland B, Smith JL, et al. CBFA2T3-GLIS2 model of pediatric acute megakaryoblastic leukemia identifies FOLR1 as a CAR T cell target. *J Clin Investig*. 2024;134(16):e184305.
36. Cairns J, Freire-Pritchett P, Wingett SW, et al. CHiCAGO: robust detection of DNA looping interactions in capture Hi-C data. *Genome Biol*. 2016;17(1):127.
37. Gopalakrishnan S, Van Emburgh BO, Shan J, et al. A novel DNMT3B splice variant expressed in tumor and pluripotent cells modulates genomic DNA methylation patterns and displays altered DNA binding. *Mol Cancer Res*. 2009;7(10):1622—1634.
38. Gress V, Roussy M, Boulianne L, et al. CBFA2T3::GLIS2 pediatric acute megakaryoblastic leukemia is sensitive to BCL-XL inhibition by navitoclax and DT2216. *Blood Adv*. 2024;8(1):112—129.
39. Kaushal A, Roy Choudhury S. SET-NUP214-induced hypermethylation landscape promotes abnormal overexpression of *HOXC* cluster genes in acute megakaryoblastic leukemia. *Genes Dis*. 2025;12(2):101320.
40. Malinge S, Chlon T, Doré LC, et al. Development of acute megakaryoblastic leukemia in Down syndrome is associated with sequential epigenetic changes. *Blood*. 2013;122(14):e33—e43.
41. Smith J, Sen S, Weeks RJ, Eccles MR, Chatterjee A. Promoter DNA hypermethylation and paradoxical gene activation. *Trends Cancer*. 2020;6(5):392—406.
42. Martinez-Sarmiento JA, Cosma MP, Lakadamyali M. Dissecting gene activation and chromatin remodeling dynamics in single

human cells undergoing reprogramming. *Cell Rep*. 2024;43(5):114170.
43. Kiani K, Sanford EM, Goyal Y, Raj A. Changes in chromatin accessibility are not concordant with transcriptional changes for single-factor perturbations. *Mol Syst Biol*. 2022;18(9):e10979.
44. Masetti R, Pigazzi M, Togni M, et al. CBFA2T3-GLIS2 fusion transcript is a novel common feature in pediatric, cytogenetically normal AML, not restricted to FAB M7 subtype. *Blood*. 2013;121(17):3469—3472.
45. Hagelkruys A, Sawicka A, Rennmayr M, Seiser C. *The Biology of HDAC in Cancer: The Nuclear and Epigenetic Components. Histone Deacetylases: The Biology and Clinical Implication*. Berlin, Heidelberg: Springer; 2011:13—37.
46. Barneda-Zahonero B, Parra M. Histone deacetylases and cancer. *Mol Oncol*. 2012;6(6):579—589.
47. Zhou Y, Jin X, Yu H, et al. HDAC5 modulates PD-L1 expression and cancer immunity via p65 deacetylation in pancreatic cancer. *Theranostics*. 2022;12(5):2080—2094.
48. Lee G, Joo JC, Choi BY, Lindroth AM, Park SJ, Park YJ. Neuroprotective effects of Paeonia Lactiflora extract against cell death of dopaminergic SH-SY5Y cells is mediated by epigenetic modulation. *BMC Complement Altern Med*. 2016;16:208.
49. Masalmeh RHA, Taglini F, Rubio-Ramon C, et al. *De novo* DNA methyltransferase activity in colorectal cancer is directed towards H3K36me3 marked CpG islands. *Nat Commun*. 2021;12(1):694.
50. So JY, Skrypek N, Yang HH, et al. Induction of DNMT3B by PGE2 and IL6 at distant metastatic sites promotes epigenetic modification and breast cancer colonization. *Cancer Res*. 2020;80(12):2612—2627.
51. Wong KK. DNMT1: a key drug target in triple-negative breast cancer. *Semin Cancer Biol*. 2021;72:198—213.
52. Rhee I, Bachman KE, Park BH, et al. DNMT1 and DNMT3b cooperate to silence genes in human cancer cells. *Nature*. 2002;416(6880):552—556.